Fuel 95 (2012) 257–262

Contents lists available at SciVerse ScienceDirect

Fuel

journal homepage: www.elsevier.com/locate/fuel

Iron oxide nanoparticles for rapid adsorption and enhanced catalytic oxidation of thermally cracked asphaltenes

Nashaat N. Nassar *, Azfar Hassan, Lante Carbognani, Francisco Lopez-Linares, Pedro Pereira-Almao

Department of Chemical & Petroleum Engineering, Schulich School of Engineering, University of Calgary, Calgary, Alberta, Canada T2N 1N4

ARTICLE INFO

Article history:
Received 5 July 2011
Received in revised form 23 August 2011
Accepted 8 September 2011
Available online 22 September 2011

Keywords:
Athabasca vacuum residue
Catalyst
Fe_3O_4
Oxidation
Mass transfer adsorption

ABSTRACT

Thermally cracked asphaltenes from Athabasca vacuum residue produced at four different process severities were investigated for adsorption and subsequent catalytic oxidation. Fe_3O_4 nanoparticles were used for the removal of these four different thermally cracked asphaltenes from toluene solutions by a batch-adsorption technique followed by subsequent catalytic oxidation. Asphaltene adsorption kinetics and isotherms are presented. Further, the catalytic effect of nanoparticles on asphaltene oxidation has been addressed. Adsorption was rapid as equilibrium was achieved within 10 min. The equilibrium adsorption data fit well to the Langmuir model. It was found that the adsorption rate, affinity and capacity depend on the molecular weight (MW) of the asphaltenes. Adsorption rate and capacity were highest for the lower MW molecules while adsorption affinity was strongest for the larger MW molecules. In addition, in the absence of nanoparticles, the four thermally cracked asphaltenes oxidized differently. However, when adsorbed onto Fe_3O_4 nanoparticles their oxidation behavior became similar, showing the enhanced catalytic effect of nanoparticles.

1. Introduction

With the rapid increase in global demand for energy and with the continuous declining in conventional oil resources, focus on world unconventional oil resources, like oilsands, to meet energy demands has increased tremendously [1]. Oilsands is a mixture of bitumen (heavy oil), water, sand and clay. Heavy oil/bitumen recovery from oilsands, with current processes, is more water and energy intensive [2]. The oilsands must be heated before bitumen can be recovered for processing. Further, upgrading heavy oil/bitumen requires more complex technologies than for conventional crude oil [3]. Actually, the presence of heavy polar hydrocarbons in bitumen makes upgrading challenging and costly, as well as a significant source of CO_2 emissions. Therefore, the development of new, cost-effective and carbon-efficient technologies is crucial for oilsands extraction and exploration processes in meeting the environmental regulations. To this end, research on nanotechnology for heavy oil upgrading by asphaltene removal, air emission capture and wastewater treatment becomes relevant [4–9]. Because of their unique properties, such as high surface area to volume ratio, high degree of dispersion, excellent adsorption affinity and catalytic activity, nanoparticles can be used to positively impact the oilsands industry with a cost-effective and more environmental approach [4]. Our long-term research objective is to separate the unstable heavy polar hydrocarbons by adsorbing them onto a solid adsorbent-catalyst. These selectively separated hydrocarbon compounds would then be used to produce hydrogen via catalytic steam gasification, which is different than conventional gasification and would operate at significantly lower temperatures [3]. In this case, hydrogen would be produced from the most difficult-to-process asphaltenes rather than natural gas, a clean fuel that could better be used for heat and power in order to displace coal. However, before pilot plant or field test performance, the adsorption affinity and catalytic activity of the nanoparticles towards thermally cracked asphaltenes have to be determined. This study aimed at investigating the adsorption kinetics and isotherms of thermally cracked asphaltenes onto Fe_3O_4 nanoparticles and identified the important variables governing the interaction of these species with nanoparticles. Furthermore, the effect of nanoparticles towards catalytic oxidation of thermally cracked asphaltenes was also investigated. This study provides potential application for iron oxide nanoparticles for heavy oil recovery and catalytic upgrading, which could be a viable alternate clean technology.

2. Experimental

2.1. Materials

Nanoparticles of Fe_3O_4 were obtained from Nanostructured and Amorphous Materials, Inc., Houston, TX. The particle size, specific

* Corresponding author. Tel.: +1 403 210 9772; fax: +1 403 210 3973.
E-mail address: nassar@ucalgary.ca (N.N. Nassar).

0016-2361/$ - see front matter © 2011 Elsevier Ltd. All rights reserved.
doi:10.1016/j.fuel.2011.09.022

surface area (BET) and external surface area of the nanoparticles were 22 ± 1.5 nm, 43 and 37 m^2/g, respectively. Particle size was determined by using X-ray Ultima III Multi Purpose Diffraction System (Rigaku Corp., The Woodlands, TX) with Cu Kα radiation operating at 40 kV and 44 mA with a θ–2θ goniometer. Surface areas of the nanoparticles were measured by a surface area and porosity analyzer (TriStar II 3020, Micromeritics Corporate, Norcross, GA). Surface area was measured by performing N_2-adsorption–desorption at 77 K. The sample was degassed at 150 °C under N_2 flow overnight before analysis. Specific surface area was calculated using Brunauer–Emmet–Teller (BET) equation and the external surface area was determined by *t*-plot method. Clearly, no significant difference was observed between the surface areas obtained by BET and *t*-plot methods, suggesting that the nanoparticles are non-porous. *n*-heptane (HPLC grade, Sigma–Aldrich) and toluene (Spectrophotometric grade, Sigma–Aldrich) were used for asphaltene isolation and model heavy oil solution preparation, respectively. A vacuum residue from Athabasca bitumen provided by Suncor was employed in this work. This feedstock contains 26 wt% distillable fractions (> 545 °C), as determined by high temperature simulated distillation (SimDist). An amount of about 0.7 wt% of methylene chloride, insoluble materials, was determined to be present within the sample. Visbroken residues, obtained through a mild thermal cracking process, at different conversion levels were prepared following a procedure developed in our previous study [10]. The corresponding visbroken asphaltenes (VBASP) were obtained by *n*-heptane precipitation, without further washing with the alkane precipitant [11]. Four types of asphaltenes having different molecular weight were prepared. The samples were labeled as VBASP6, VBASP7, VBASP8 and VBASP9; with VBASP9 having the lowest molecular weight. Accordingly, individual heavy oil model solutions were prepared by dissolving the corresponding VBASP in toluene. All chemicals were used without further purification.

2.2. Size exclusion chromatography

The asphaltenes molecular weights (MW) were estimated by size exclusion (liquid) chromatography (SEC). One PL-Gel Minimix-E column, Tetrahydrofuran (THF) eluent and differential refractive index detection were set up for these analyses. More details on the analysis procedure can be found elsewhere [11]. The main properties of the considered visbroken asphaltenes are summarized in Table 1. It should be noted that the molecular sizes of the selected asphaltenes were roughly estimated based on the determined parameters from SEC analyses. One important feature that must be considered for thermal cracked asphaltenes is their increased aromaticity, ranging in the present case from 0.43 for virgin asphaltenes to 0.60 for severely cracked asphaltenes (VBASP9). From the SEC determined parameters presented in Table 1, the average molecular representations containing from 260 carbon atoms for virgin asphaltenes down to 64 carbon atoms for severely cracked asphaltenes were estimated. Their aromatic regions comprise from 113 down to 38 carbon atoms per average molecular representation. Alkyl appendages also decrease in length from changes brought by thermal cracking.

2.3. Elemental analysis

Solid asphaltenes samples were analyzed for C, H elemental contents with a LECO analyzer. N and S elemental contents were determined for known toluene sample solutions (ca. 10 wt%) with an ANTEK 9000 analyzer. The elemental composition for the studied asphaltenes is presented in Table 1.

2.4. Adsorption kinetic experiments

Adsorption kinetic experiments were carried out with a Cary 4 UV–Vis spectrophotometer (Varian Technon Pty Ltd. Australia) by selecting a wavelength of 303 nm for monitoring purposes [12]. 300 mg of Fe_3O_4 nanoparticles were added to a 1 cm quartz cuvette containing 3 mL model heavy oil solution at 83 ± 4 mg/L asphaltene concentration and 296 K. The sample was shaken manually every 3 min for 10 s and accordingly the change of absorbance for asphaltenes in the supernatant was recorded continuously for every 3 min up to 42 min.

2.5. Equilibrium adsorption isotherms

Batch adsorption experiments were conducted for the four types of asphaltenes at 298 K with initial concentration in the range of 200–3000 mg/L. All experiments were conducted in 25 ml tightly sealed vials. The nanoparticle dosage was fixed at 100 mg, and the volume of the sample solution was 10 mL. To ensure complete equilibrium, the samples were agitated at 200 rpm by placing them in a temperature incubator for 24 h. The nanoparticles containing adsorbed asphaltenes were removed from the suspension by a small horseshoe Alnico magnet, and the supernatant was decanted. The residual concentration of the asphaltenes in the supernatant was measured by UV–Vis spectrophotometry. The adsorbed amount of asphaltenes onto nanoparticles (mmol of asphaltenes/g of dry nanoparticles) was calculated as:

$$Q_e = \frac{C_o - C_e}{m} V \tag{1}$$

where Q_e is the equilibrium adsorbed amount of asphaltenes (mmol/g), V is the volume of solution (L), m is the dry mass of nanoparticles (g), C_o is the initial concentration of asphaltenes in the solution (mmol/L) and C_e is the equilibrium concentration of asphaltenes in the solution (mmol/L).

2.6. Adsorption modeling

Adsorption isotherms of different types of asphaltenes onto nanoparticles were modeled using the Freundlich and Langmuir models presented in Eqs. (2) and (3), respectively.

$$Q_e = Q_m \frac{K_L C_e}{1 + K_L C_e} \tag{2}$$

$$Q_e = K_F C_e^{1/n} \tag{3}$$

where K_L is the Langmuir equilibrium adsorption constant related to the affinity of adsorption (L/mmol), Q_m is the maximum adsorbed amount of asphaltenes per mass of nanoparticles for complete

Table 1
Properties of the selected visbroken asphaltenes.

Type of asphaltenes	Log (MW)	H (wt%)	C (wt%)	N (wt%)	H/C (atomic ratio)	S (wt%)	Max. estimated molecular size (nm)[a]
VBASP6	3.31	8.58	78.35	0.86	1.31	8.65	4.5
VBASP7	3.30	7.69	80.69	0.98	1.14	8.59	4.5
VBASP8	2.95	7.32	81.76	0.99	1.07	6.79	2.1
VBASP9	2.96	7.55	81.83	1.05	1.11	6.08	2.1

[a] For virgin asphaltenes: 6.0 nm.

monolayer coverage (mmol/g), K_F is the Freundlich constant related to the adsorption capacity ((mmol/g)(L/mmol)$^{1/n}$), and $1/n$ is the adsorption intensity factor (unitless). The Freundlich and Langmuir constants were estimated by minimization of the sum of squares of the differences between the experimental value and the predicted one. The optimization was conducted by using the Solver feature in Excel. The non-linear Chi-square analyses were conducted for comparing the best-fit-model as per Eq. (4) [13].

$$\chi^2 = \sum \frac{(Q_{exp} - Q_{Model})^2}{Q_{Model}} \quad (4)$$

where Q_{exp} and Q_{Model} are the equilibrium adsorbed amount of asphaltenes obtained experimentally and from modeling, respectively.

2.7. Thermogravimetric analysis

Catalytic oxidation of adsorbed thermally cracked asphaltenes over Fe_3O_4 nanoparticles was carried out and studied using a simultaneous thermogravimetric analysis/differential scanning calorimetry (TGA/DSC) analyzer (SDT Q600, TA Instruments, Inc., New Castle, DE). Thermogravimetric analyses of thermally cracked asphaltenes, fresh Fe_3O_4 nanoparticles, and Fe_3O_4 nanoparticles containing adsorbed asphaltenes were conducted for comparison. About 5–10 mg of the sample was heated under air atmosphere. The flow rate of air was kept at 100 cm^3/min. The samples were heated to 800 °C at a heating rate of 10 °C/min.

3. Results and discussions

3.1. Adsorption kinetics

Fig. 1a–d shows the results obtained in the kinetic studies on visbroken asphaltene adsorption onto Fe_3O_4 nanoparticles. The figure represents the adsorbed amount of asphaltenes as a function of time for initial asphaltene concentration of 83 ± 4 mg/L at a set up temperature of 296 K. It can be seen that, for all cases, the adsorption was fast as the adsorbed amount increased rapidly during the first 10 min and remained unchanged after 42 min of contact. This indicates that the state of equilibrium was almost reached within 10 min. This fast asphaltene adsorption is certainly related to the high dispersion degree of nanoparticles as well as the high availability of external surface area, as the selected Fe_3O_4 is a nonporous adsorbent [4], hence, it takes very little time for the molecules to be adsorbed, as a result of the absence of intra-particle diffusion that limits the adsorption rate. The adsorption rate for the different asphaltenes was estimated from the slope of line at the beginning of each curve presented in Fig. 1a–d. The values of the adsorption rate are presented in Fig. 2. The kinetic efficiency, represented by adsorption rate value, for different asphaltenes follows the order VBASP9 > VBASP8 > VBASP7 > VBASP6.

3.2. Adsorption isotherms

Fig. 3a and b shows that, for all the four types of asphaltenes, adsorption increased at low equilibrium concentration and starts to level off at higher concentration, suggesting that Fe_3O_4 nanoparticles have good adsorption affinity for all the types of asphaltenes with a possibility of monolayer coverage. The equilibrium adsorption of the four types of asphaltenes onto nanoparticles was modeled using the Langmuir and Freundlich models. Table 2 summarizes the estimated Langmuir and Freundlich parameters for the four types of asphaltenes. As seen in Table 2, the estimated χ^2 values of the Langmuir model are smaller than the ones of the Freundlich model. Therefore, the Langmuir model is the best-fit model for the experimental results, suggesting that the asphaltene adsorption occurs on a homogeneous surface by monolayer adsorption.

The differences in the adsorption of the four asphaltenes are illustrated by comparing the maximum adsorption capacities and adsorption affinities. Fig. 4 shows the values of adsorption capacity and adsorption affinity in terms of the Langmuir constants, Q_m and K_L, respectively. The adsorption capacity followed the order VBASP9 > VBASP8 > VBASP7 > VBASP6. This is in well agreement with the findings pertaining to the adsorption performance of different asphaltenes on the basis of the kinetic efficiency, represented by adsorption rate. Interestingly, the adsorption affinity

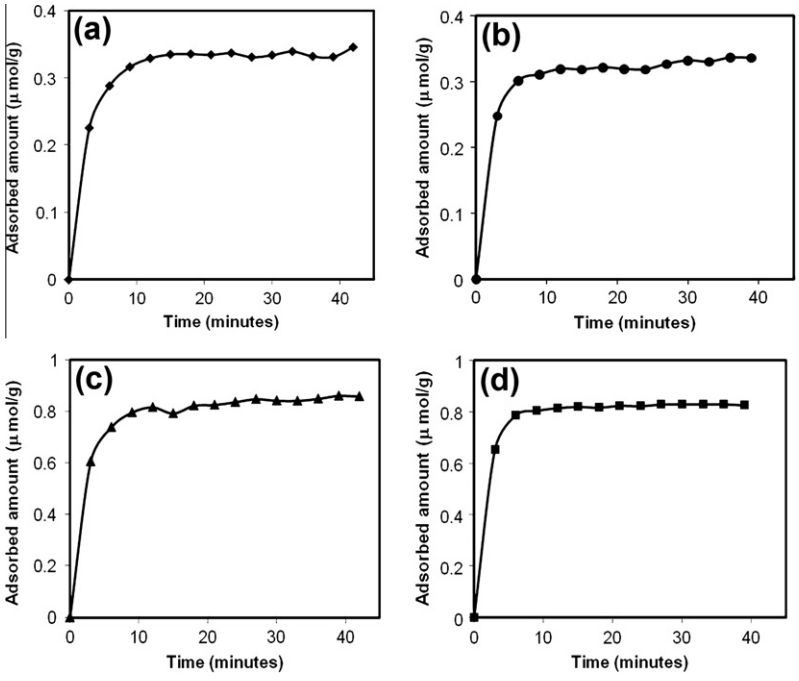

Fig. 1. Adsorption kinetics of: (a) ATVB6, (b) ATVB7, (c) ATVB8 and (d) ATVB9 onto Fe_3O_4 nanoparticles obtained at initial concentration of 83 ± 4 mg/L and 296 K.

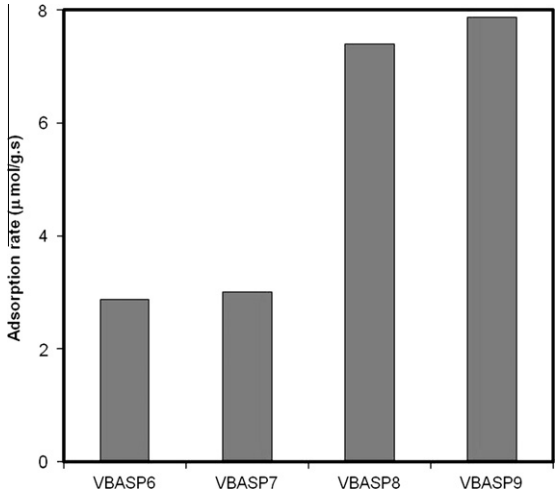

Fig. 2. Estimated values of the adsorption rate for different types of visbroken asphaltenes onto Fe_3O_4 nanoparticles at 296 K.

follows a reversed order. These order differences can be attributed to a different degree of interaction between iron oxide surface and the type of asphaltenes. It has been reported that iron oxide interacts strongly with asphaltenes and resin hydrocarbon group types, and hence affects their H-bonding tendency and increases their retentive properties [14].

In order to determine the adsorption performance as well as the molecular parameters that govern the adsorption, correlations between Q_m and log MW of the asphaltenes, its H/C atomic ratio (aromatic character), nitrogen content and sulfur content were carried out. These correlations are presented in Fig. 5. As seen, low MW asphaltenes, which are believed to have more aromatic character (Low H/C) and high nitrogen content, are more prone to interact effectively with the iron-based nanoparticles. This is not surprising as in our previous study we found that the adsorption of those types of asphaltenes over solid surfaces is enhanced by low H/C ratio (more aromatic character) and high nitrogen content [11,15,16]. The results presented here indicate that an increase in the aromatic nature of asphaltenes increases the molecular interaction between the π electrons of aromatic ring with Fe. Also

Table 2
Langmuir and Freundlich isotherm parameters for the four thermally cracked asphaltenes obtained at 298 K.

Asphaltene	Freundlich model			Langmuir model		
	K_F (mmol/g)(L/mmol)$^{1/n}$	$1/n$ (unit less)	χ^2	K_L (L/mmol)	Q_m (mmol/g)	χ^2
VBASP 6	0.062	0.406	0.003	17.03	0.047	0.003
VBASP 7	0.069	0.476	0.0017	12.27	0.048	0.0005
VBASP 8	0.068	0.438	0.0007	3.77	0.085	0.0002
VBASP 9	0.096	0.646	0.0015	1.07	0.197	0.0016

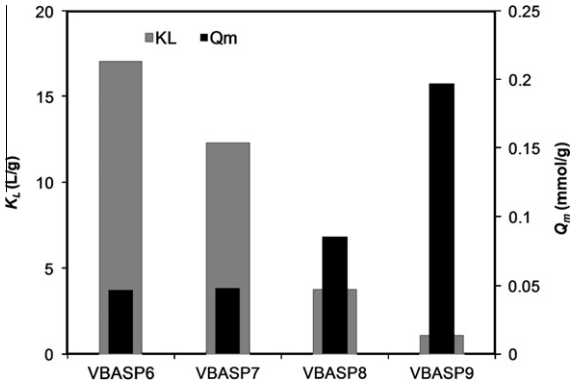

Fig. 4. Adsorption affinity (K_L) and adsorption capacity (Q_m) for different types of visbroken asphaltenes onto Fe_3O_4 nanoparticles.

bonding of N atoms with Fe cannot be ruled out, if asphaltene molecules align parallel to the metal surface in a face up position [17]. Accordingly, higher N content in severely cracked asphaltenes would favor adsorption. It is worth noting that this N content contains both, basic and non-basic nitrogen compounds, which may interact differently with the nanoparticles. For instance, iron compounds are prone for the selective adsorption of basic type nitrogen (pyridinic) rather than non-basic (pyrrolic) [18]. Nonetheless, it should be noted that, in the current study, the total N content

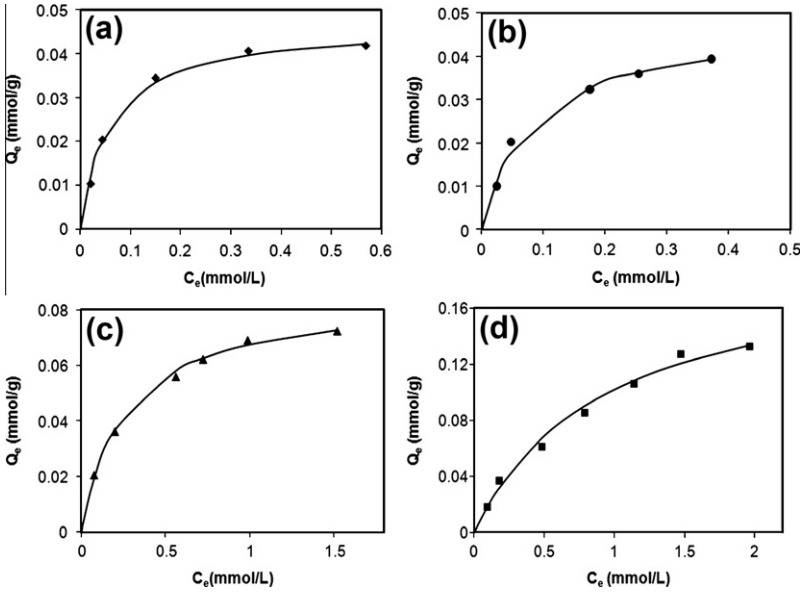

Fig. 3. Adsorption isotherms of: (a) VBASP6, (b) VBASP7, (c) VBASP8 and (d) VBASP9 onto Fe_3O_4 nanoparticles at 298 K. Points are experimental data and the solid lines are from the Langmuir isotherm model (Eq. (2)).

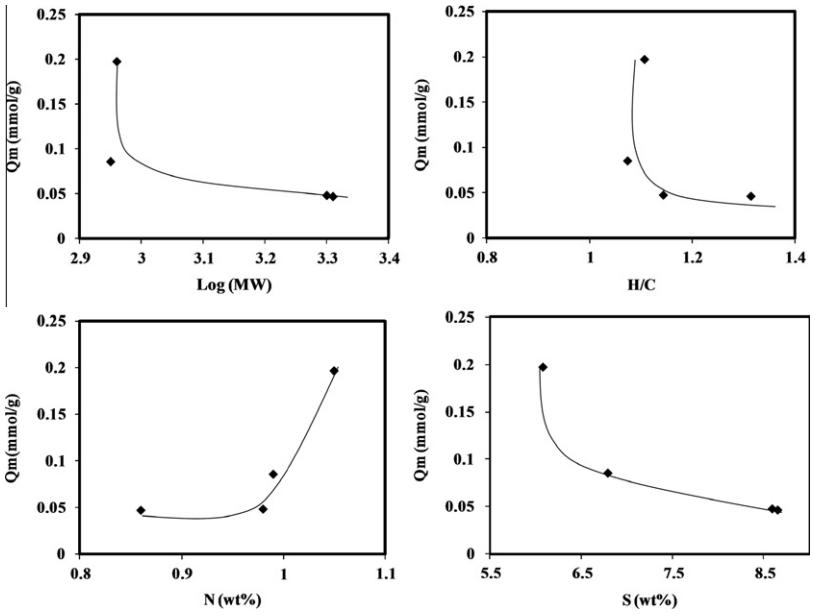

Fig. 5. Correlations between Q_m and Log MW, H/C, N and S content.

did not vary significantly in the first three fractions of thermally cracked asphaltenes, and only the most thermally cracked molecule has appreciable N content. Therefore, a study on relative fraction of basic and non-basic N compounds was not deemed significant for the selected four types of visbroken asphaltenes. As for the S content, it appears that asphaltene uptake increased as the S content decreased. This decrease in the content of S with the decrease in the molecular weight of asphaltenes is attributed to the loss of alkyl moieties linked to the asphaltene structure through S-linkages (e.g., sulfide and/or disulfide bridges) that are removed easily by thermal cracking, and hence led to a decrease in S content. This would leave a nucleus that interact easily with the nanoparticles and thus facilitate the adsorption [15].

3.3. Catalytic oxidation of adsorbed visbroken asphaltenes

Catalytic oxidation of asphaltenes was performed to obtain valuable insight on the catalytic effect of the Fe_3O_4 nanoparticles toward the different types of visbroken asphaltenes using a thermogravimetric setup. Thermogravimetric analysis was conducted

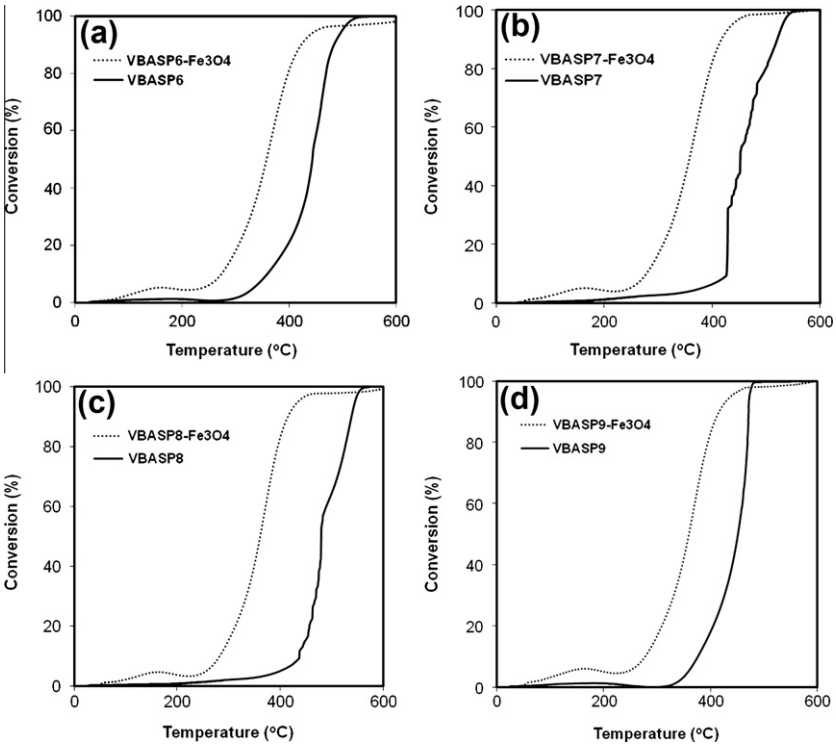

Fig. 6. Percent conversion of: (a) ATVB6, (b) ATVB7, (c) ATVB8 and (d) ATVB9 in oxidation with presence or absence of Fe_3O_4 nanoparticles.

to determine the sample mass loss when heated in air, with linear increase in temperature. Reactivity of bulk visbroken asphaltenes toward oxidation before adsorption onto nanoparticles was also tested for comparison. Percent conversion ratio (α) was determined from the mass loss data as follows:

$$\alpha = \frac{m_o - m_t}{m_o - m_\infty} \quad (5)$$

where m_o is the initial sample mass, m_∞ is the final sample mass and m_t is the sample mass at any time. Figs. 6a–d shows plots of percent conversion ratio (α) of the four types of visbroken asphaltenes in the presence and absence of Fe_3O_4 nanoparticles as a function of temperature. It appears that oxidation of bulk visbroken asphaltenes depends on their properties, however, no systematic trends have been determined so far. All the four types of asphaltenes have different oxidation temperature for the start and maximum percent conversion. However, in the presence of Fe_3O_4 nanoparticles the four types of asphaltenes showed identical conversion rate and oxidation temperature. Fe_3O_4 nanoparticles greatly enhanced the oxidation process, depicting catalytic effect of the considered nanoparticles. For all asphaltenes, the oxidation process started at about 220 °C with nanoparticles instead of about 380–400 °C in the absence of the nanoparticles. This decrease in temperature for oxidation reaction clearly shows the catalytic behavior of Fe_3O_4 nanoparticles toward asphaltenes oxidation. As a result, the activation energies required for the oxidation reactions of asphaltenes in the presence and absence of Fe_3O_4 nanoparticles were calculated by using the thermal analysis data following the method developed by Coats and Redfern [19]. The estimated average activation energy of visbroken asphaltenes was approximately 82.5 kJ/mol. In the presence of Fe_3O_4 nanoparticles, the average activation energy was 55.8 kJ/mol. From the above mentioned results, it is evident that the presence of Fe_3O_4 nanoparticles caused a drop in the oxidation temperature and average activation energy, hence showing their catalytic effect.

4. Conclusions

Fe_3O_4 nanoparticles were employed for adsorptive and oxidation removal of four different visbroken asphaltenes obtained from thermally cracked vacuum residue. Adsorption kinetics showed that equilibrium was practically achieved in less than 10 min. Decreasing the asphaltene molecular weight favored the adsorption rate. The adsorption isotherm of the four asphaltenes onto Fe_3O_4 nanoparticles was Langmuir type, suggesting monolayer coverage. It was found that the extent of adsorption increased with decrease in the molecular weight of the asphaltenes. However adsorption affinity increased as the molecular weight of asphaltenes increased. The presence of Fe_3O_4 nanoparticles with asphaltenes caused a significant decrease in the oxidation temperature and average activation energy, depicting high catalytic activity. This study shows that Fe_3O_4 nanoparticles can serve as an excellent adsorbent/catalyst for heavy oil upgrading provided that an effective method of nanoparticles separation followed by adsorbed asphaltene gasification is to be implemented.

Acknowledgments

Financial support provided by Carbon Management Canada, Inc. (CMC-NCE), a research network financed by the National Science and Engineering Research Council (NSERC), is gratefully acknowledged.

References

[1] Tanaka N. World energy outlook 2010. Jakarta: International Energy Agency; 2010.
[2] Government of Alberta. Environmental management of Alberta's oilsands; 2009. Available from: http://environment.gov.ab.ca/info/library/8042.pdf (accessed 1.5.2011).
[3] Nassar NN, Hassan A, Pereira-Almao P. Application of nanotechnology for heavy oil upgrading: catalytic steam gasification/cracking of asphaltenes. Energy Fuels 2011;25:1566–70.
[4] Nassar NN, Hassan A, Pereira-Almao P. Metal oxide nanoparticles for asphaltene adsorption and oxidation. Energy Fuels 2011;25:1017–23.
[5] Nassar NN, Pereira-Almao P. Capturing H_2S(g) by in situ-prepared ultradispersed metal oxide particles in an oilsand-packed bed column. Energy Fuels 2010;24:5903–6.
[6] Nassar NN, Husein MM, Pereira-Almao P. Ultradispersed particles in heavy oil: part II, sorption of H2S(g). Fuel Process Technol 2010;91:169–74.
[7] Nassar NN. Kinetics and equilibrium studies on the adsorptive removal of nickel, cadmium and cobalt from wastewater by superparamagnetic iron oxide nanoadsorbents. Can J Chem Eng 2011.
[8] Nassar NN. Rapid removal and recovery of Pb(II) from wastewater by magnetic nanoadsorbents. J Hazard Mater 2010;184:538–46.
[9] Nassar NN. Kinetics, mechanistic, equilibrium, and thermodynamic studies on the adsorption of acid red dye from wastewater by γ-Fe_2O_3 nanoadsorbents. Sep Sci Technol 2010;45:1092–103.
[10] Carbognani L, Gonzalez MF, Pereira-Almao P. Characterization of Athabasca vacuum residue and its visbroken products. Stability and fast hydrocarbon group-type distributions. Energy Fuels 2007;21:1631–9.
[11] López-Linares F, Carbognani L, Sosa-Stull C, Pereira-Almao P, Spencer RJ. Adsorption of virgin and visbroken residue asphaltenes over solid surfaces. 1. Kaolin, smectite clay minerals, and athabasca siltstone. Energy Fuels 2009;23:1901–8.
[12] González MF, Stull CS, López-Linares F, Pereira-Almao P. Comparing asphaltene adsorption with model heavy molecules over macroporous solid surfaces. Energy Fuels 2007;21:234–41.
[13] Montgomery DC, Runger GC. Applied statistics and probability for engineers. 4 ed. New York: John Wiley & Sons; 2006.
[14] Carbognani L. Effects of iron compounds on the retention of oil polar hydrocarbons over solid sorbents. Pet Sci Technol 2000;18:335–60.
[15] Lopez-Linares F, Carbognani L, Hassan A, Pereira-Almao P, Rogel E, Ovalles C et al. Adsorption of athabasca vacuum residue and their visbroken products over macroporous solids: influence of their molecular characteristics. Energy Fuels; 2011 doi: 10.1021/ef201047z.
[16] López-Linares F, Carbognani L, Spencer RJ, Pereira-Almao P. Adsorption studies in Athabasca core sample: virgin and mild thermal cracked residua. Energy Fuels 2011;25:3657–62.
[17] Ortega-Rodriguez A, Alvarez-Ramirez F, Cruz SA, Lira-Galeana C. A model to calculate the average interaction energy and adhesion force between petroleum asphaltenes and some metallic surfaces. J Colloid Interface Sci 2006;301:352–9.
[18] Habeeb JJ. Method for selectively removing basic nitrogen compounds from lube oils using transition metal halides and transition metal tetrafluoroborates. CA 1172195. Canada; 1984.
[19] Coats AW, Redfern JP. Kinetic parameters from thermogravimetric data. Nature 1964;201:68–9.